Advances in Geo-Energy Research

Vol. 17, No. 1, p. 56-67, 2025

Original article

Nanostructure and evolution of thin shells in brittle-ductile shear zones

Zhourong Cai[1], Yuqi Liu[1], Jianfeng Li[2], Yan Sun[3]*

[1]*School of Marine Sciences, Sun Yat-sen University, Zhuhai 519082, P. R. China*

[2]*Guangzhou Institute of Geochemistry, Chinese Academy of Sciences, Guangzhou 510640, P. R. China*

[3]*School of Earth Sciences and Engineering, Nanjing University, Nanjing 210093, P. R. China*

Keywords:
Nanostructure
evolution
thin shell
brittle shear zone
ductile shear zone

Cited as:
Cai, Z., Liu, Y., Li, J., Sun, Y. Nanostructure and evolution of thin shells in brittle-ductile shear zones. Advances in Geo-Energy Research, 2025, 17(1): 56-67.
https://doi.org/10.46690/ager.2025.07.05

Abstract:
The brittle-ductile deformation of rocks forms the foundation of structural geology, engineering geology and petroleum geology. Although brittle-ductile deformation structures and their evolutionary processes have been extensively investigated at macroscopic and microscopic scales, a reliable discrimination model remains elusive at the nanoscale. To establish distinctive nanostructural models for brittle-ductile deformations, this study combines the scanning electron microscopy analysis of thin shells within brittle-ductile shear zones with high-temperature and high-pressure experimental simulations. The brittle and ductile thin shell models exhibit markedly different structures. The models reveal a tripartite architecture in brittle thin shells: a vice-surface on top layer; a middle layer comprising individual spherical nanoparticles, nanoparticle aggregates and multi-aggregate nanoparticles; a basal substrate layer. In contrast, the ductile thin shell does not have a vice-surface on top layer or a basal substrate layer and its nanostructures are characterized by fibrous, chain-ball and schistose nanoparticles with their associated aggregate structures. Applying the space-for-time assumption, the evolution of thin shells in the shear zone was reconstructed, demonstrating that the brittle-ductile-viscous transition drives nanoparticle transformations through granularization - alienation - reuniting - reproduction sequences. This work extends the discrimination model of brittle-ductile deformation from the microscopic scale to the nanoscale.

1. Introduction

Investigating the brittle-ductile deformation of rocks represents a fundamental area of research in structural geology that emerged in the late 1960s, though it initially predominantly focused on the macroscopic and mesoscopic scales (Ramsey, 1968; Mitra, 1979; Means, 1984). Brittle deformation refers to the process where rocks suddenly rupture due to stress exceeding the strength limit under the conditions of low temperature, low confining pressure and high pore pressure. Ductile deformation, on the other hand, refers to the continuous deformation achieved by intragranular plastic flow (such as dislocation slip) or mineral recrystallization in rocks under high temperature and high confining pressure conditions (Obert and Duvall, 1967; Hucka and Das, 1974). Brittle-ductile deformation is the basis for solving many geological problems, including those in oil & gas exploration, thus it exhibits significant application value. Brittle deformation facilitates the formation of hydrocarbon reservoirs, whereas ductile deformation tends to form seals that impede further hydrocarbon migration. With the advent of unconventional reservoirs (e.g., shale gas and tight oil), studies of brittle-ductile deformation at the microscale and beyond are increasingly critical.

At the macroscopic level, brittle shear zones and ductile

*Corresponding author.
E-mail address: caizhr@mail.sysu.edu.cn (Z. Cai); liuyq99@mail2.sysu.edu.cn (Y. Liu); ljf@gig.ac.cn (J. Li); sunyan37@sina.com (Y. Sun).
Yandy Scientific Press
2207-9963
Received May 19, 2025; revised June 12, 2025; accepted June 27, 2025; available online July 1, 2025.

shear zones exhibit distinct characteristics and are relatively straightforward to differentiate (Anders and Wiltschko, 1994). Brittle shear zones are characterized by fracture surfaces and associated cataclasites, whereas ductile shear zones primarily manifest as continuous plastic deformation without fracture surfaces (Miranda et al., 2020; Boffadossi et al., 2021; Sun and Dong, 2023). The method for discriminating between brittle and ductile deformation remains applicable at the microscopic scale, hence the brittle-ductile transition has been studied more extensively (Buergmann and Pollard, 1992; Ju et al., 2003; Fusseis et al., 2006; Viti and Collettini, 2009). At this scale, the two types of deformation can be differentiated by examining the mineralogical composition, grain size distribution, dynamic recrystallization processes, metamorphic reactions, microfracture patterns, and other microstructural deformation features of rocks (Fusseis and Handy, 2008; Mamtani et al., 2023; Zhan et al., 2023).

Brittle-ductile deformation generates nanoparticles whose fundamental physicochemical properties markedly differ from those observed at the macroscopic and microscopic scales (Ju et al., 2022). Consequently, the brittle-ductile deformation at the nanoscale exhibits greater complexity, representing an intricate interplay between structural elements (spatial factors) and diagenetic processes (temporal factors) (Dill, 2010) while also being influenced by nanofabrication arrays (Krása et al., 2009). Although significant research has been conducted on nanoscale brittle-ductile deformation along fault sliding surfaces (Di Toro et al., 2006; De Paola, 2013; Siman-Tov et al., 2013; Verberne et al., 2014) and ductile and shear zones (Sun et al., 1992; Cai et al., 2019; Sun and Dong, 2023), the scientific community still lacks a viable discrimination model to differentiate between brittle and ductile deformation within shear zones at the nanoscale.

Thin shell (or film) developed within the shear zones, which constitutes the focus of this research, provides an ideal natural laboratory for probing brittle-ductile deformation at the nanoscale. Essentially, a layer of silicification (or calcification) forms on the shear sliding surface with a thickness less than 1 cm (the thickness of nanolayer is less than 1 μm), which is called a dynamic thin shell or shear thin shell (Sun et al., 1992; Chester et al., 1993; Wibberley and Shimamoto, 2003; Smith et al., 2011; Fondriest et al., 2012). It is the strip with the highest shear stress, the most intense strain and the most developed nanostructure. In brittle shear zones, thin shells are the smooth surfaces of faults, whereas in ductile shear zones, they comprise the foliation (potential fracture surfaces) formed by the directional arrangement of minerals (Sun et al., 2008a, 2013). To this end, this study investigates the nanostructural characteristics and evolutionary processes of thin shells within exhumed brittle-ductile shear zones. Through combined field observations and HTHP experimental verification, we aimed to establish a comprehensive discrimination model for nanoscale brittle-ductile deformation.

2. Materials and methods

2.1 Field sampling and analysis

The Tan-Lu Fault Zone in Eastern China, the Median Tectonic Line in Central Japan, and the San Andreas Fault Zone in Western USA collectively constitute major components of a circum-Pacific strike-slip megabelt. In contrast, the Red River Fault Zone in Western China represents a continental-scale strike-slip system resulting from the collision between the Indian and Eurasian Plates. These major fault systems share comparable evolutionary histories and mechanical characteristics, having all experienced significant shear sliding deformation. Rock samples were collected from the southern segment of the Tan-Lu Fault Zone in the Xishanyi area of Anhui Province (Fig. 1(a)). Following detailed regional geological analysis, this work specifically targeted two representative shear zones: (1) A brittle shear zone developed in Mesozoic granite (Fig. 1(b)), and (2) a ductile shear zone within marble of the Proterozoic Feidong Group (Pt_{2f}) (Fig. 1(c)) for oriented sampling. Field investigations revealed that Mesozoic granite outcrops are pervasively mantled by cataclastic rocks. These exposures exhibit well-developed shear-slip surfaces characterized by prominent slickensides and densely spaced striations, providing compelling evidence for predominant brittle shear deformation (Fig. 1(b)). In contrast, the Proterozoic Feidong Group outcrops develop clear mylonitic foliation and no significant brecciation or open fracture is observed, indicating that ductile shear deformation is dominant (Fig. 1(c)).

2.2 Sample observation methods

The samples were initially observed using optical microscopy for preliminary characterization. Following this initial screening, representative specimens meeting strict selection criteria were chosen for detailed analysis using a Scanning Electron Microscope (SEM) (type LEO-1530VP).

Before observation, samples were broken into thin slices of 5×5 mm, strapped with conductive adhesive tape and fixed the exposed surfaces to the sample bench. According to occurrence measurement, the directions of the specimen and fabric axes a, b and c (where a is parallel to the shearing direction, $b \perp a$ and $c \perp ab$) were determined. Then, metal spraying equipment was used for 140 s at a current of 20 mA to create a metal film of 1 nm in size onto the observation surface of the sample. This procedure enhances the conductivity of the sample observation surface and improves the SEM observation effect. Normally, the accelerating voltage (HV) was set at 15.00 KV.

2.3 HTHP experiments

The microdeformation characteristics of the fault surface under different temperatures and pressures were simulated through High-Temperature and High-Pressure (HTHP) experiments. The Paterson-type High-Temperature and High-Pressure Deformation Apparatus (HTPDA), installed at the Guangzhou Institution of Geochemistry, Chinese Academy of Sciences, was designed to study the deformation of materials from Earth under HTHP conditions (Fig. 2) (Li et al., 2021). The HTPDA mainly consists of a high-pressure vessel, a high-temperature furnace and an axial motor for applying compre-

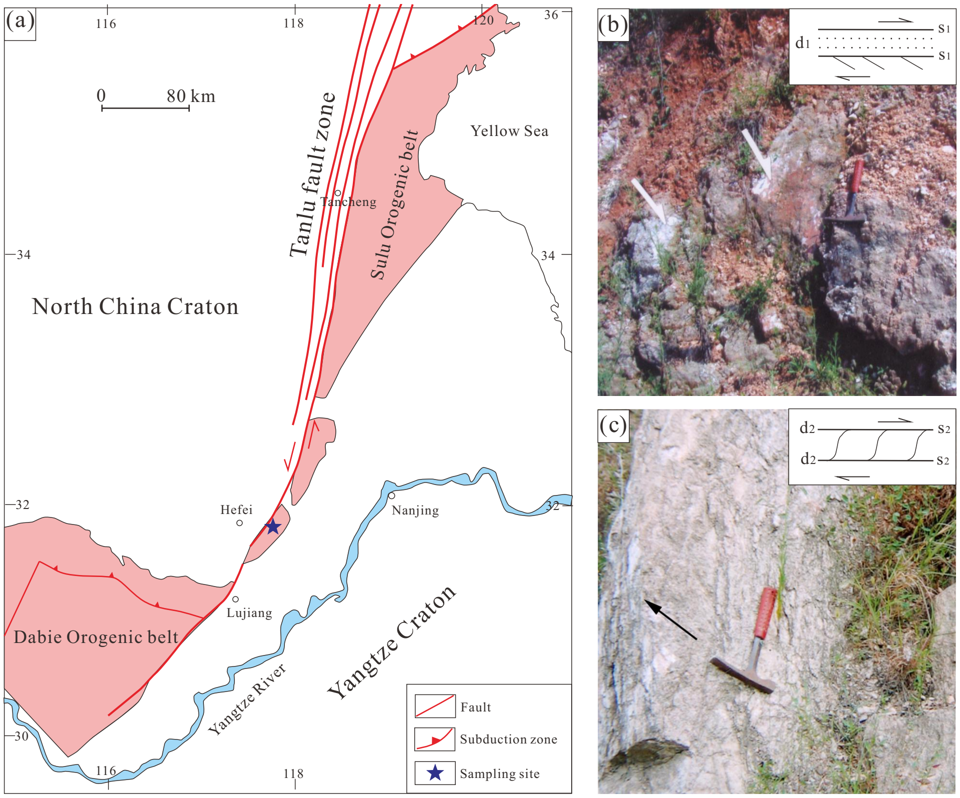

Fig. 1. Sampling position of brittle and ductile shearing fault zones. (a) Simplified diagram of the regional structure at the sampling location (modified after Cheng et al. (2017)), (b) brittle shearing fault zone developed in granite, with the arrow showing a sampling point of the shear thin shell and a sketch of cross section (the upper right) indicating shear slipping (arrow) planes (s1) and shear thin shell (d1) and (c) Ductile shearing fault zone developed in marble, with the arrow showing a sampling point of the shear schistosity zone and a sketch of cross section (the upper right) indicating shear slipping (arrow) planes (s2) and shear thin film (d2).

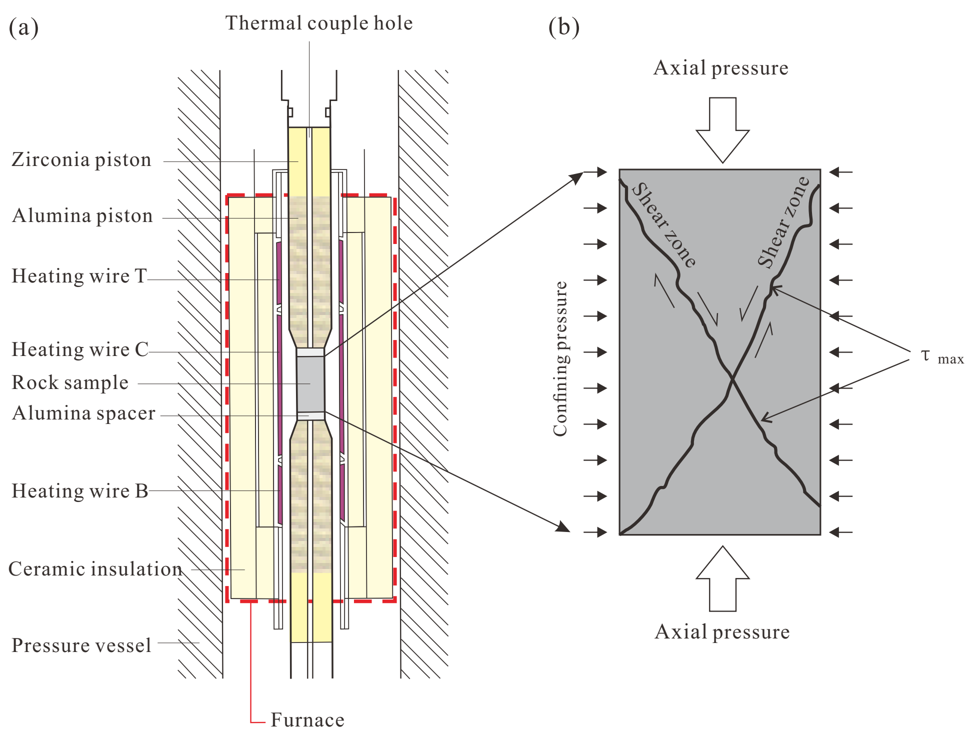

Fig. 2. (a) Axial deformation experimental arrangement of the HPTDA and (b) schematic diagram of sample deformation forming shear zones.

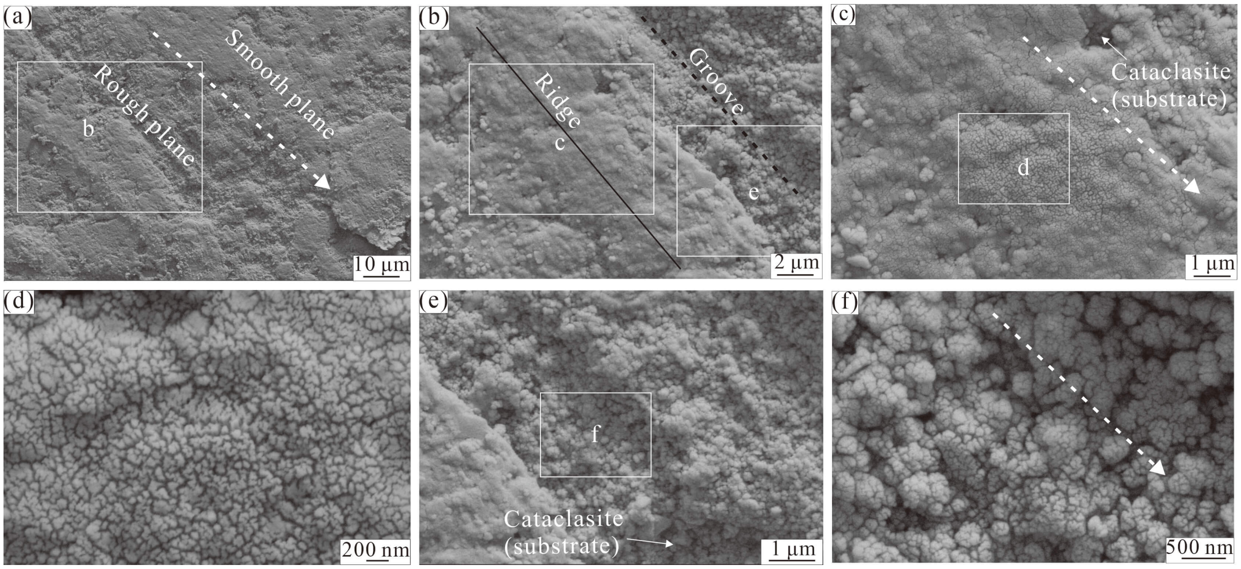

Fig. 3. SEM images of the thin shell in brittle shear zone. (a) Scratches, ridges and grooves can be seen on the thin shell, indicating the direction of movement (white dotted arrow), (b) the smooth plane (vice-surface, sliding ridge) and the rough plane (sliding groove), (c)-(d) the nanostructures of the smooth plane on the thin shell, where the nanoparticles are densely arranged in layers and (e)-(f) the nanostructures of the rough plane on the thin shell, where the spherical individual nanoparticles and nanoparticle aggregates are distributed randomly.

Table 1. Testing condition and mechanical results under HTHP conditions.

Sample		Confining pressure (MPa)	Temperature (°C)	Maximum differential stress (MPa)	Strain capacity (%)
Granite	A1	200	27	510	1.8
	A2	200	600	570	3.1
	A3	200	700	180	1.7
Marble	B1	30	27	260	8.8
	B2	60	27	330	9.1
	B3	90	27	400	10.6
	B4	120	27	440	10.1
	B5	150	27	480	11.8
	B6	180	27	510	11.7

ssion/deformation. The machine uses Ar gas as the confining medium, and a pressure range of 0.1 ~ 500 MPa can be experimentally simulated by two-level pressurization. The high-temperature module adopts a built-in three-unit winding furnace and can simulate a temperature environment from room temperature to 1,300 °C. For more information on the HTPDA, refer to the literature (Paterson, 1970).

To better verify the observation results of the field samples, two series of experiments were conducted: One was to simulate the brittle shear deformation with granite samples and the other was to simulate the ductile deformation with marble samples.

After the experiments, from the axial displacement data of the internal force recorded in real time by a computer connected to the machine, the nominal strain, differential stress and strain rate of the samples could be obtained. The temperature and confining pressure settings and maximum differential stress results for each deformation experiment are shown in Table 1. To ensure that the samples reached a certain differential stress before undergoing shear fracture, a confining pressure of 200 MPa was set in the granite samples. Two samples were studied at 600 °C and 700 °C, respectively, to check whether the nanoparticles would aggregate at high temperatures. Different confining pressures were set for the marble samples to determine the development of nanoparticles under different confining pressures (or differential stresses).

The samples were cut after the HTHP experiments and observed by SEM (ZEISS Ultra 55) at the Experimental Center of the South China Normal University.

3. Results and analysis

3.1 Nanostructure analysis in brittle shear deformation

Cataclastic rocks are widely developed within brittle fault zones (Fig. 1(a)) and exhibit well-defined slickenside planes and densely concentrated slickenside lines on shear surfaces. SEM observations revealed that slickensides can be classified into two distinct morphological types: Smooth planes and rough planes (Figs. 3(a) and 3(b)). The smooth plane represents a secondary surface developed on the shear thin shell, corresponding to the tribological concept of vice-surface (or secondary texture) (Durham et al., 2002). In contrast, the rough plane constitutes the original surface of the thin shell that becomes exposed through either mechanical damage or

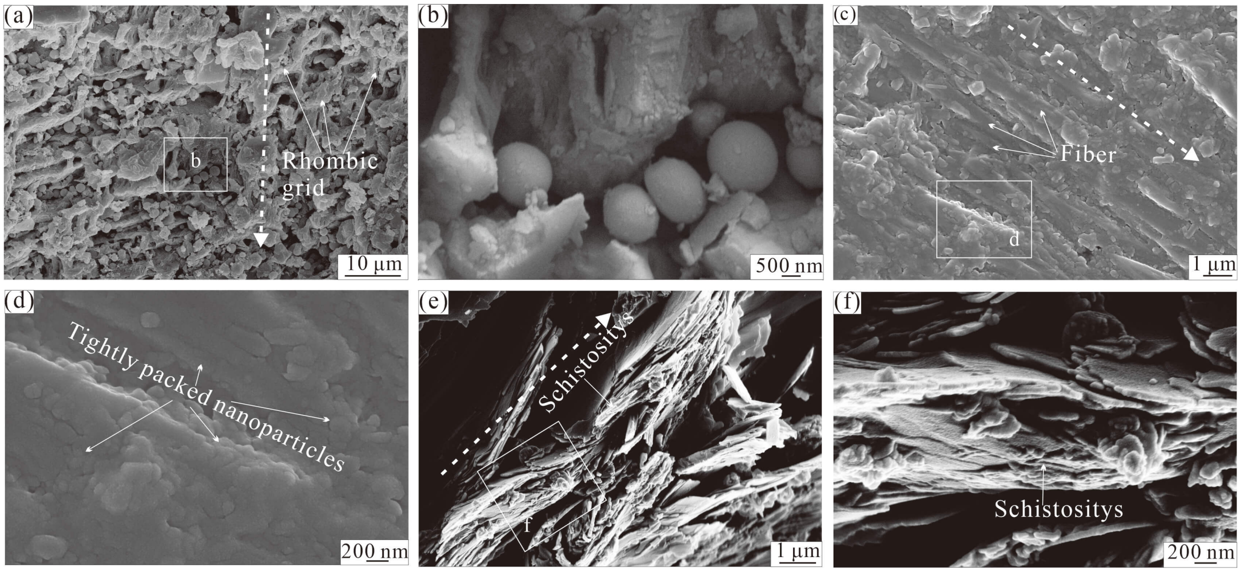

Fig. 4. SEM images of the thin shell on ductile shear zone. (a)-(b) Rhombic grid-like nanostructure, (c)-(d) fibrous or chainball-shaped nanostructure. (e)-(f) schistose nanostructure. The white dotted arrow indicates the direction of ductile shear.

incomplete development of the vice-surface (Figs. 3(b)-3(d)). Importantly, all observed slickenside features (including both smooth and rough planes) consistently preserve kinematic indicators that record the slip direction. At the nanometer-scale resolution, slickenside lines can be further categorized into sliding ridges and sliding grooves, with euritic grains (substrate) frequently occurring within groove bottoms (Figs. 3(c) and 3(e)).

Both the smooth plane (usually corresponding to sliding ridges) and rough plane (usually associated with sliding grooves) exhibit distinctive nanostructural characteristics. The smooth plane manifests as a nanoscale-thickness film containing a high density of both individual nanoparticles and nanoparticle aggregates. These nanoparticles demonstrate well-defined layered arrangements (Figs. 3(c) and 3(d)) and exhibit clear evidence of plastic isomerization (Keulen et al., 2007; Sun et al., 2008b). In contrast, the rough plane is characterized by numerous individual spherical nanoparticles and spherical nanoparticle aggregates, which display irregular spatial distributions (Figs. 3(e) and 3(f)).

3.2 Nanostructure analysis in ductile shear deformation

Shear schistosity is extensively developed within the ductile shear deformation zone, forming potential fracture surfaces. The nano-scale shear thin shells investigated in this study are located on the surfaces of shear schistosity. The nanostructures of shear thin shells in the ductile shear deformation zone can be categorized into three types (Fig. 4).

The first type is characterized by a rhombic grid-like structure (Figs. 4(a) and 4(b)). This grid consists of fibers formed by the dense arrangement of nanoparticles. The orientation of these fibers indicates the direction of ductile shear deformation (Fig. 4(a)). Additionally, numerous pores are observed within the grid, with some spherical nanoparticles filling these pores (Fig. 4(b)).

The second structural type exhibits either fibrous or chainball-shaped morphology (Figs. 4(c) and 4(d)). These fibers display a characteristic ridge-and-groove pattern with dense alignment, clearly marking the orientation of ductile shear deformation (Fig. 4(c)). High-magnification observations reveal that the fibrous structures consist of tightly packed nanoparticles, while certain regions show sparsely distributed nanoparticles forming distinctive chainball configurations (Fig. 4(d)).

The third structural type manifests as a well-defined schistose fabric (Figs. 4(e) and 4(f)). This consists of multiple layers exhibiting staggered stacking patterns, with locally developed tear and fold structures within the schistosity. The orientation of schistosity planes is a reliable indicator of the direction of ductile shear deformation (Fig. 4(e)). Nanoscale examination reveals that the schistose boundaries are characterized by well-aligned nanoparticle arrays (Fig. 4(f)).

The thin shell structures developed in ductile shear deformation zones (including rhombic grid-like, fibrous, chainball-like, and schistose morphologies) demonstrate characteristic features consistent with superplastic deformation mechanisms (Verberne et al., 2014), and these structural patterns fundamentally differ from those observed in brittle shear deformation zones.

3.3 Nanostructure analysis of shear deformation in other areas

To further validate the above findings, comparative SEM analyses were conducted on samples collected from brittle shear zones and ductile shear zones in other fault zones. These investigations revealed consistent nanostructural patterns analogous to those previously described (Fig. 5). Specifically, in the northern section of the Red River strike-slip fault zone, brittle shear thin shells exhibited distinct nanoscale features

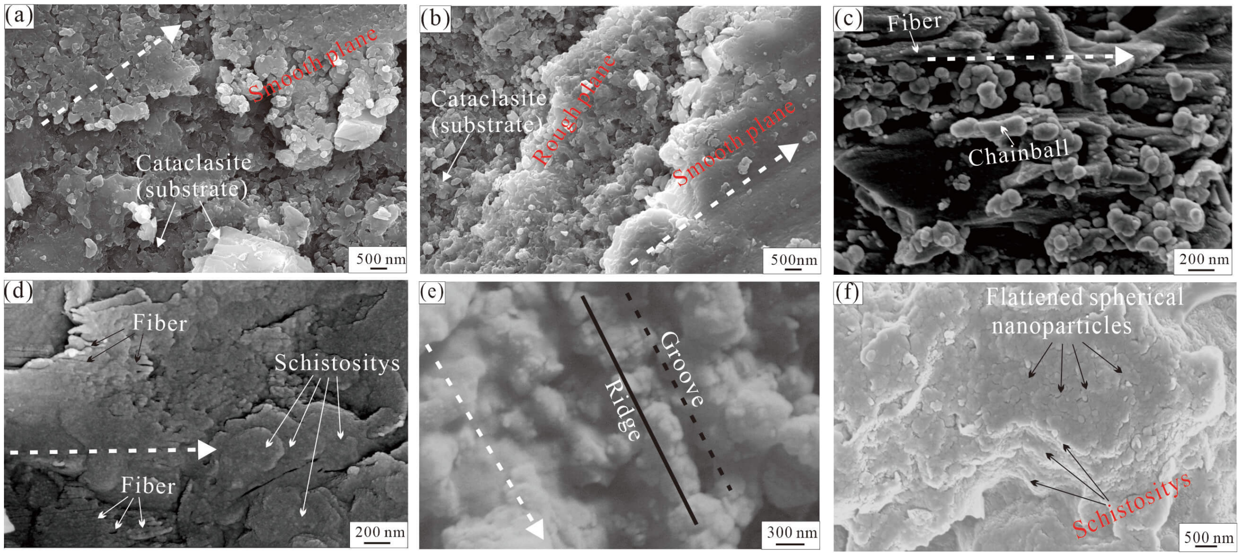

Fig. 5. SEM images of nanostructure in other brittle or ductile shear zones. (a)-(b) Nanostructure of the thin shell of the brittle shear zone in the northern section of the Red River strike-slip fault zone, (c)-(d) nanostructure of the thin shell of the ductile shear zone in the central section of the Red River strike-slip fault zone, (e) nanostructure of the thin shell of brittle shear fault growing in Triassic formation at the Mufushan, Nanjing suburbs and (f) nanostructure of the thin shell of the ductile shear zone developing in the Tan Lu fault zone of Shandong Province section. The white dotted arrow indicates the direction of shear.

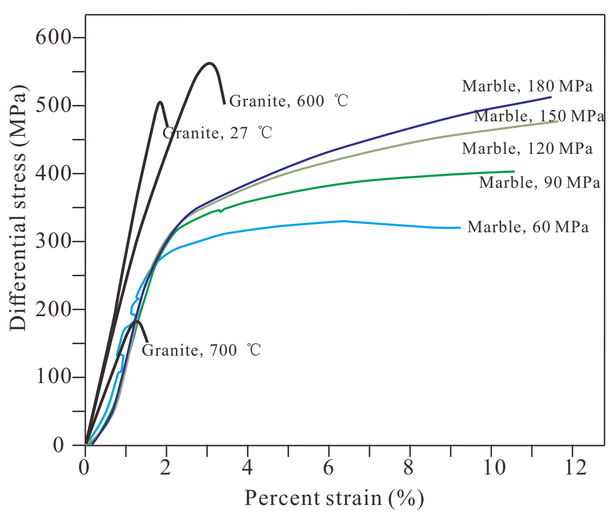

Fig. 6. Differential stress versus percent strain curve.

including (1) contrasting smooth and rough surface morphologies, and (2) both individual and aggregated nanoparticle arrangements (Figs. 5(a) and 5(b)). Conversely, ductile shear thin shells from the middle section of the Red River strike-slip fault zone displayed characteristic fibrous, chainball-like, and schistose nanostructures (Figs. 5(c) and 5(d)). Additional observations from the Mufushan Triassic formation (Nanjing) showed aggregated nanoparticles with ridge-groove textures in brittle shear zones (Fig. 5(e)), while schistose nanostructures were identified in ductile shear zones along the Shandong section of the Tan-Lu fault system (Fig. 5(f)).

SEM observations demonstrated significant nanoscale distinctions between brittle and ductile shear deformation. Brittle deformation is manifested as discrete nanoparticles (or nanoparticle aggregates). In contrast, ductile deformation consistently exhibits continuous nanostructural patterns, such as interconnected nanogrids, aligned nanofibers, and spherical nanochainballs. These diagnostic nanostructural differences have been systematically observed across various shear zone environments, suggesting fundamental differences in deformation physics at the nanoscale.

3.4 Results of HTHP experiments

The differential stress-strain curves (Fig. 6) demonstrate distinct deformation behaviors between the tested lithologies. All three granite specimens exhibited brittle failure at strains below 3%, as evidenced by sudden stress drops in the loading curves. In contrast, the four marble samples maintained structural integrity beyond 10% strain, displaying characteristic ductile deformation patterns without macroscopic rupture. Through these experimental results, the primary objective of replicating fundamental brittle-ductile deformation behaviors under controlled laboratory conditions was successfully achieved.

The experimental samples were observed and analysed at the microscopic and nanoscales. In the brittle deformation of granite (Fig. 7), it can be seen that the mineral particles inside the granite are in a disordered state before the experiment (Fig. 7(a)), while after the experiment, they are arranged in an ordered manner and some minerals have undergone deformation, such as mica and feldspar (Fig. 7(b)). Under SEM, the experimental samples exhibited deformation characteristics (Figs. 7(c) and 7(d)) similar to those of the exhumed brittle shear zone (Figs. 3 and 5). On the fractured surface of granite experimental samples, smooth and rough surfaces can be observed, as well as the euritic grains in the bottom

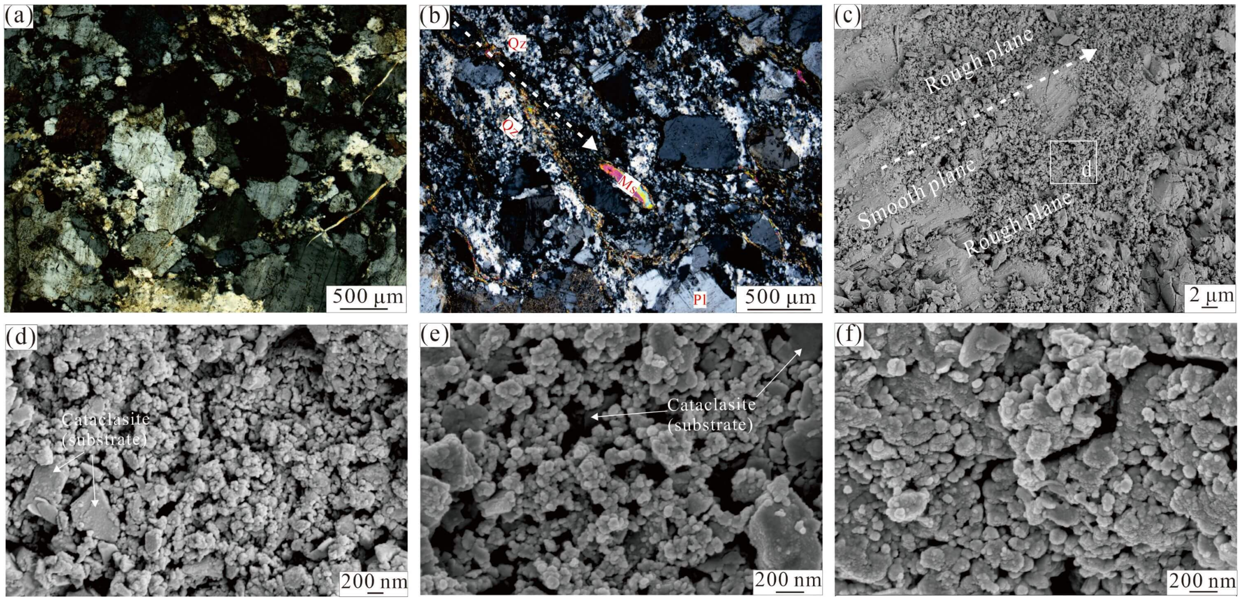

Fig. 7. Observation results in brittle fracture deformation experiments of granite. (a) Microscopic characteristics of granite sample before the experiment, (b) microscopic characteristics of granite samples after the experiments (confining pressure of 200 MPa, temperature of 27 °C), (c) characteristics of granite samples under SEM (confining pressure with 200 MPa, temperature of 27 °C), (d) a local magnification of (c), (e) characteristics of granite samples under SEM (confining pressure of 200 MPa, temperature of 600 °C) and (f) characteristics of granite samples under SEM (confining pressure of 200 MPa, temperature of 700 °C). The white dotted arrow indicates the direction of brittle shear. Note: Qz, quartz, Ms, muscovite, Pl, plagioclase.

(Fig. 7(c)). However, the surface is not as smooth as that in the exhumed brittle shear zone. The reason is that the experiment stops immediately once the sample breaks and the sliding distance is very short. A large number of individual spherical nanoparticles can be seen on the rough plane (Fig. 7(d)). In the experiments with relatively high temperatures of 600 and 700 °C, a large number of aggregated nanoparticles developed on the fracture surface (Figs. 7(e) and 7(f)), which indicates that the morphology of nanoparticles is related to temperature. Individual nanoparticles are prone to form at low temperatures, while aggregated nanoparticles are prone to form at high temperatures.

Experiments with marble demonstrated the characteristics of ductile shear deformation. Before the experiment, the calcite particles in the marble were relatively uniform and the arrangement had no obvious pattern under the microscope (Fig. 8(a)). After the experiment, the arrangement of calcite showed a certain orientation, and some calcites had some fracture surfaces (Fig. 8(b)). During the experiments, the confining pressures were set at 60, 90, 150 and 180 MPa, respectively; however, at the nanoscale, there was no significant difference in the internal structure of marble. A large number of fibrous or chainball-like nanoparticles developed inside the marble samples after the four experiments, indicating the direction of ductile shear deformation. The fibers and chainballs were inlaid with spherical nanoparticles (Figs. 8(c)-8(f)). These experimental results are consistent with the results observed on the exhumed ductile shear zone.

4. Discussion

4.1 Models of nanostructure within thin shells

The SEM observation of shear zones (Figs. 3-5) and the results of HTHP experiments (Figs. 7 and 8) revealed the clear nanostructure of the thin shells on the brittle-ductile deformation zone.

The thin shell structure in the brittle shear deformation zone can be divided into five layers: a1-e1 (Fig. 9(a)). Layer a1 is primary rock that does not show the characteristics of brittle deformation. Layer b1 is commonly cataclastic rock or a series of cataclastic-granulitic rock. Layers a1 and b1 do not develop nanoparticles and do not have a nanodeformation structure, serving as the basement of the thin shell. Granulitic grains and nm/μm grains mingle with each other in layer c1, and loose grains lightly present a direct arrangement (Siman-Tov et al., 2013). Layer c1 is the substrate layer of nanostructure in brittle thin shells (Figs. 3(c), 3(e), 5(a), 5(b), 7(d) and 7(e)), while layer d1 is a mixed layer of individual nanoparticles and aggregate nanoparticles. Individual nanoparticles have relevant roundness, sphericity and irregular arrangement (De Paola, 2013; Cai et al., 2019). The aggregate nanoparticles with different degree isomerization concentrate into the aggregate grains and multi aggregate grains (Figs. 3(e) and 3(f)). Layer e1 is the top layer of the thin shell, which possesses a smooth plane (vice-surface). It is formed by the re-compaction and deformation of individual or aggregate nanoparticles (Figs. 3(a), 3(c), 3(d), 5(a), 5(b) and 7(c)). The undeformed individual or aggregate nanoparticles form

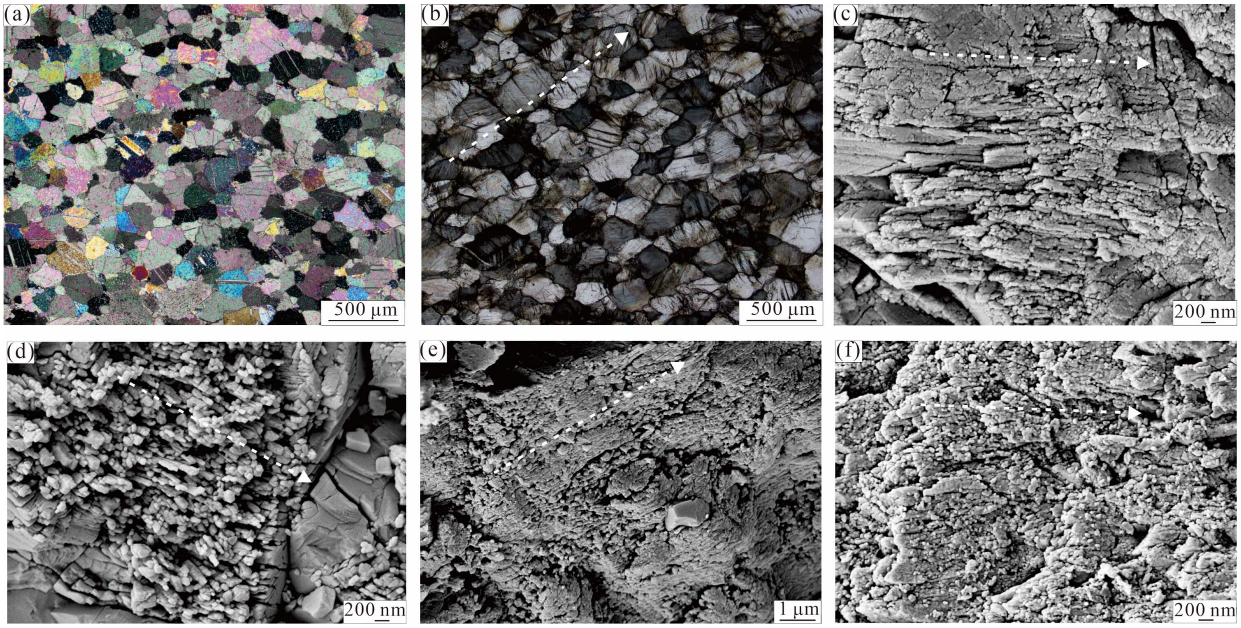

Fig. 8. Observation results in ductile deformation experiments of marble. (a) Microscopic characteristics of marble sample before the experiments, (b) microscopic characteristics of marble sample after the experiments (confining pressure of 200 MPa), (c) characteristics of marble sample under SEM (confining pressure of 60 MPa), (d) characteristics of marble sample under SEM (confining pressure of 90 MPa), (e) characteristics of marble sample under SEM (confining pressure of 150 MPa) and (f) characteristics of marble sample under SEM (confining pressure of 180 MPa). The white dotted arrow indicates the direction of ductile shear.

a rough plane (Figs. 3(b), 3(e), 3(f), 5(a), 5(b) and 7(c)).

The thin shell structure in the ductile shear deformation zone can be divided into four layers: a2-d2 (Fig. 9(b)). Layer a2 is primary rock and the basement of the thin shell; Layer b2 is granulated rock, with its original morphological characteristics retained, and these particles are usually at the nanoscale and do not separate from each other. Layer c2 develops rhombic grid-like, fibrous, chainball-like or schistose nanostructures (Figs. 4, 5(c)-5(f) and 8(c)-8(f)), which exhibit superplastic deformation (Keulen et al., 2007; Sun et al., 2008b; Verberne et al., 2014). Layer d2 consists of some dispersed nanoparticle layers, including individual nanoparticles and aggregate nanoparticles (Figs. 4(a) and 4(b)). These nanoparticles are peeled off from the layer c2. Obviously, from layer b2 to d2, the strain of the thin shell keeps increasing. Layer d2 demonstrates the characteristics of brittle deformation.

The nanostructures between brittle deformation and ductile deformation have significant differences. There is a vice-surface on the top nanostructure of brittle thin shells and a substrate layer at the bottom. In contrast, the ductile thin shells lack these two structural layers. The nanoparticles of brittle thin shells are in the form of individual spherical nanoparticles, nanoparticle aggregates and multi-aggregate nanoparticles, while those of the ductile thin shells are in the form of fibrous, chain-ball and schistose nanoparticles, demonstrating stronger superplastic deformation. Overall, at the nanoscale, brittle deformation of the thin shell is characterized by discrete particle arrangements, while ductile deformation of the thin shell manifests as continuous nanostructures. The simultaneous existence of discrete nanoparticles and continuous superplastic nanofibers represents the brittle-ductile transition at the nanoscale. A detailed comparison between brittle deformation and ductile deformation of the thin shells is shown in Table 2.

4.2 Evolution of nanostructure within thin shells

The nanostructural characteristics observed in thin shells at both the brittle and ductile shear zones not only reveal distinct structural units but also serve as significant indicators of two fundamentally different deformation evolutions. The models of brittle-ductile deformation in thin shells (Fig. 9) demonstrate a strain gradient from bottom to top (from a1 to e1 at Fig. 9(a) and from a2-d2 at Fig. 9(b)), which can be used to reconstruct the evolution of thin shells in shear zones. This method is called space-for-time assumption, where space can be used as a proxy for time to investigate the evolution of brittle and ductile shear zones (Mitra, 1979; Means, 1984; Ingles, 1986; Watterson, 1986; Hull, 1988; Carreras, 2001; Fusseis et al., 2006; Fusseis and Handy, 2008). Under the condition of gradually increasing strain, the deformation of brittle shear zone and ductile shear zone develops along two different pathways, respectively (Fig. 10). Under identical strain conditions, the intrinsic mechanical properties of the rock play a decisive role.

In the brittle shear deformation zone, the original rocks rupture rapidly and form cataclastic rocks, which constitute the substrate layer of the brittle thin shells (Braun and Naumovets, 2006) (Figs. 9(a) and 10(a)). Subsequent strain accumulation drives the ultramylonitization of cataclasites at the

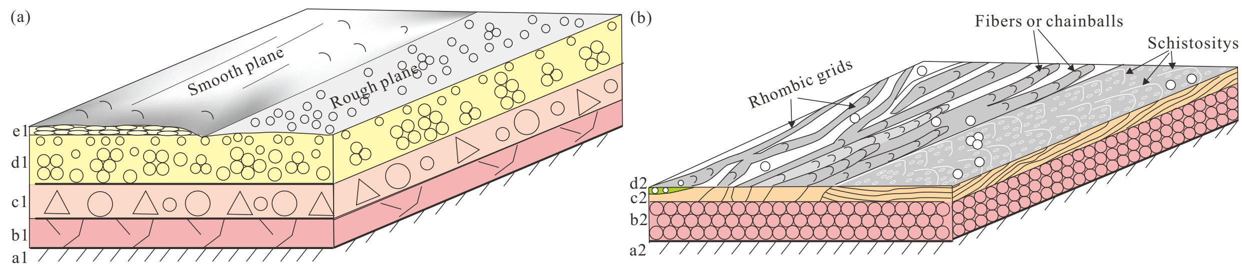

Fig. 9. Models of nanostructure in the brittle and ductile shear zones. (a) Models of nanostructure in the brittle shear zones and (b) models of nanostructure in the ductile shear zones.

Table 2. Comparative analysis of nanostructures at the brittle shear zone and ductile shear zone.

Nanostructures of thin shell					Kinematic process		
Item	Thickness of thin shell	Substrate	Vice layer	Nanoparticles of structure	Mechanical transition	Frictional mechanics	Sliding mode
Brittle shear zone	mm-cm	Present (Figs. 9(a)(c1))	Present (Figs. 9(a)(e1))	smooth plane (sliding ridge) and rough plane (sliding groove), individual spherical nanoparticles and aggregate nanoparticles	Brittle-viscous → viscous-elastic → ductile-viscous	Kinematic friction	Stick slip
Ductile shear zone	µm–cm	None	None	Rhombic grid-like, fibrous, chainball-like or schistose nanostructures	Brittle-viscous → ductile-viscous → viscous-elastic	Static friction	Creep (smooth) slip

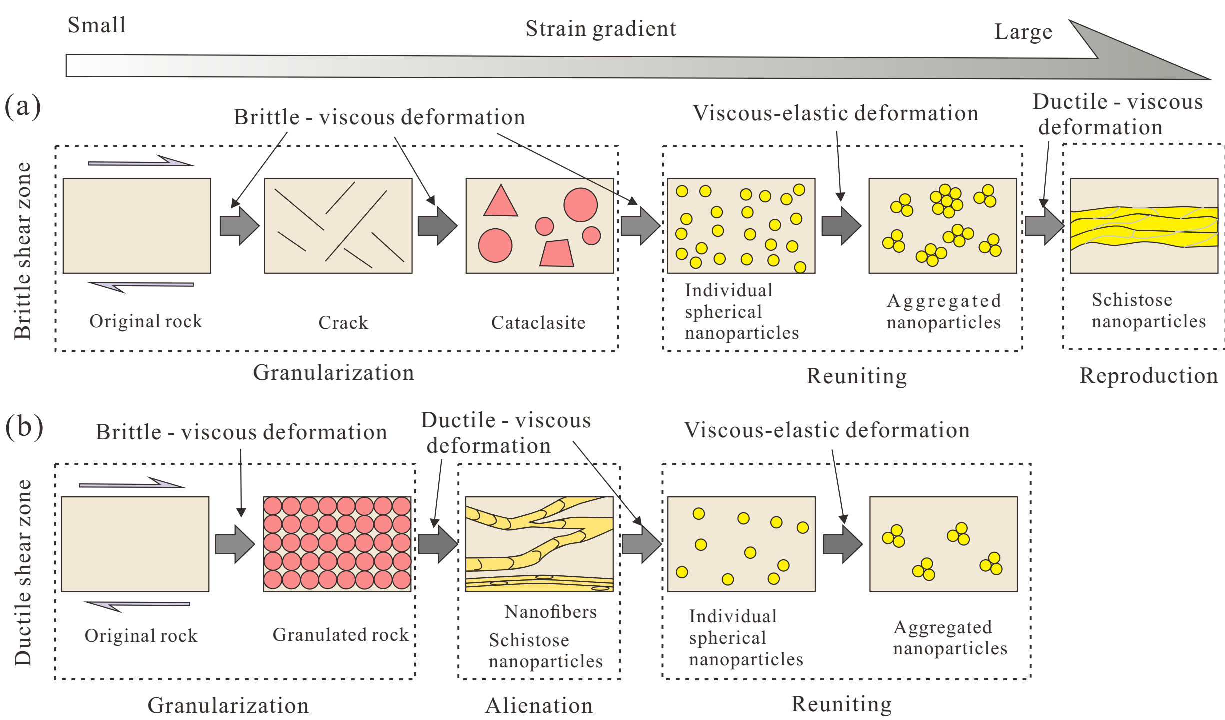

Fig. 10. Evolution of nanostructure in the thin shells of brittle-ductile shear zones.

top of the thin shell, yielding individual nanoparticles (Keulen et al., 2007; Mair and Abe, 2008). The progressive deformation from protolith to nanoparticle formation represents a brittle-viscous transition (Fig. 10(a)). These nanoparticles exhibit enhanced ductility and viscosity, facilitating their merging into aggregate nanoparticles through viscous-elastic deformation mechanisms. When the displacement of shear sliding is large enough, individual nanoparticles and aggregate nanoparticles at the top of the thin shell will deform into schistose nanoparticles, forming a smooth surface (vice-surface) (Figs. 3(b), 5(b), 7(c), 9(a) and 10(a)). This final stage constitutes a ductile-viscous deformation regime.

Within ductile shear zones, protoliths maintain structural continuity at both macro- and microscale without fracturing, yet they undergo grain-size reduction to form granulated textures (Figs. 7(e) and 10(b)). The resultant particles exhibit negligible relative displacement while preserving the original morphological framework of the rock. This deformation mechanism represents a transitional brittle-viscous regime. With increasing strain, the granulated rock undergoes superplastic stretching, forming nanofibers, chainball-like or schistose nanoparticles (Figs. 4(e), 5(c)-5(f) and 8), and this process belongs to viscous-elastic deformation mechanisms. When the displacement of shear sliding is large enough, the spherical nanoparticles that make up the nanofibers will be separated out to form individual nanoparticles and then form aggregate nanoparticles (Figs. 9(b) and 10(b)), which undergo viscous-elastic deformation (Holdsworth, 2004; Hirose et al., 2006).

During the strain-dependent brittle-ductile deformation, nanoparticles transform among granularization - alienation - reuniting - reproduction (Fig. 10), and the transition of brittle-ductile-viscous changes mainly occurs in the narrow shear zone (Dean et al., 1995; Stewart et al., 2000; McLaren and Pryer, 2001; Sun et al., 2008b).

The formation mechanisms of nanostructures in brittle-ductile shear zones involve complex, multi-scale processes. Besides being related to strain (brittle - ductile - viscous deformation) (Hirose et al., 2006; Fusseis and Handy, 2008; Siman-Tov et al., 2013), they may also interact with the mechanisms of nanocoating (Schleicher et al., 2010; De Paola et al., 2011), dynamic differentiation (Han et al., 2007, 2011; Collettini et al., 2009; Viti and Hirose, 2010), impact loads or subcritical crack growth (Sammis and Ben-Zion, 2008), grain boundary sliding (De Paola et al., 2015), and solubilization (Tian and He, 2019).

5. Conclusions

In this paper, the nanostructure models of thin shells in brittle-ductile shear zones were constructed through SEM observations of exhumed shear zones coupled with HTHP experimental simulations, which extended the discrimination model of brittle-ductile deformation from the microscopic scale to nanoscale. The nanostructure models of thin shells showed that the top of the brittle thin shell is a vice-surface, the middle consists of individual spherical nanoparticles, aggregate nanoparticles and multi aggregate nanoparticles, and the bottom is a substrate layer. Meanwhile, fibrous, chainball-shaped and schistose nanoparticles and their aggregate nanoparticles develop in the ductile shear zone. The nanostructures between brittle thin shells and ductile thin shells exhibited significant differences. The simultaneous existence of discrete nanoparticles and continuous superplastic nanofibers represents the brittle-ductile transition at the nanoscale. The space-for-time assumption is applicable to reconstructing the evolution of brittle and ductile shear zones at nanoscale. Brittle-ductile deformation of the thin shells on the shear zones is strain-dependent deformation at the nanoscale. The transition of brittle-ductile-viscous drives a nanoparticle transformation sequence involving granularization - alienation - reuniting - reproduction.

Acknowledgements

This research was supported by grants from the National Natural Science Foundation of China (Nos. 41206035 and 42172243) and the Nature Science Foundation of Guangdong Province (Nos. 2018A030313168 and 2018B030311030). We also thank Dr. Chunchao Wang from the Nanjing Institute of Geology and Paleontology for assistance in SEM observation. Datasets and figures noted in the main text can be found in the main text.

Conflict of interest

The authors declare no competing interest.

References

Anders, M. H., Wiltschko, D. V. Microfracturing, paleostress and the growth of faults. Journal of Structural Geology, 1994, 16(6): 795-815.

Buergmann, R., Pollard, D. D. Influence of the state of stress on the brittle-ductile transition in granitic rock: Evidence from fault steps in the Sierra Nevada, California. Geology, 1992, 20(7): 645-648.

Boffadossi, M. A., Coniglio, J. E., Maffini, M. N., et al. Synkinematic interplay between felsic dykes and host rock mylonitization: How magmatism assists the formation of ductile narrow shear zones in the Sierra Chica de Córdoba, Argentina. Journal of South American Earth Sciences, 2021, 106: 103063.

Braun, O. M., Naumovets, A. G. Nanotribology: Microscopic mechanisms of friction. Surface Science Reports, 2006, 60(6-7): 79-158.

Cai, Z., Lu, L., Huang, Q., et al. Formation conditions for nanoparticles in a fault zone and their role in fault sliding. Tectonics, 2019, 38(1): 159-175.

Carreras, J. Zooming on Northern Cap de Creus shear zones. Journal of Structural Geology, 2001, 23(9): 1457-1486.

Cheng, S., Liu, Z., Wang, Q., et al. SHRIMP zircon U-Pb dating and Hf isotope analyses of the Muniushan Monzogranite, Guocheng, Jiaobei Terrane, China: implications for the tectonic evolution of the Jiao-Liao-Ji Belt, North

China Craton. Precambrian Research, 2017, 301: 36-48.

Chester, F. M., Evans, J. P., Biegel, R. L. Internal structure and weakening mechanisms of the San Andreas Fault. Journal of Geophysical Research, 1993, 98(B1): 771-786.

Collettini, C., Niemeijer, A., Viti, C., et al. Fault zone fabric and fault weakness. Nature, 2009, 462: 907-910.

Dean, G. D., Tomlins, P. E., Read, B. E. A model for nonlinear creep and physical aging in poly (viny chloride). Polymer Engineering and Science, 1995, 35(16): 1282-1289.

De Paola, N. Nano-powder coating can make fault surfaces smooth and shiny: Implications for fault mechanics? Geology, 2013, 41(6): 719-720.

De Paola, N., Hirose, T., Mitchell, T., et al. Fault lubrication and earthquake propagation in thermally unstable rocks. Geology, 2011, 39(1): 35-38.

De Paola, N., Holdsworth, R. E., Viti, C., et al. Can grain size sensitive flow lubricate faults during the initial stages of earthquake propagation? Earth and Planetary Science Letters, 2015, 431: 48-58.

Dill, H. G. The "chessboard" classification scheme of mineral deposits: Mineralogy and geology from aluminum to zirconium. Earth-Science Reviews, 2010, 100(1-4): 1-420.

Di Toro, G., Hirose, T., Nielsen, S., et al. Natural and experimental evidence of melt lubrication of faults during earthquakes. Science, 2006, 311: 647-649.

Durham, W. B., Weidner, D. J., Karato, S. I., et al. New developments in deformation experiments at high pressure. Reviews in Mineralogy and Geochemistry, 2002, 51(1): 21-49.

Fondriest, M., Smith, S. A. F., Di Toro, G., et al. Fault zone structure and seismic slip localization in dolostones: An example from the Southern Alps, Italy. Journal of Structural Geology, 2012, 45: 52-67.

Fusseis, F., Handy, M. R. Micromechanisms of shear zone propagation at the brittle-viscous transition. Journal of Structural Geology, 2008, 30(10): 1242-1253.

Fusseis, F., Handy, M. R., Schrank, C., et al. Networking of shear zones at the brittle-to-viscous transition (Cap de Creus, NE Spain). Journal of Structural Geology, 2006, 28(7): 1228-1243.

Han, R., Hirose, T., Shimamoto, T., et al. Granular nanoparticles lubricate faults during seismic slip. Geology, 2011, 39(6): 599-602.

Han, R., Shimamoto, T., Hirose, T., et al. Ultra-low friction of carbonate faults caused by thermal decomposition. Science, 2007, 316: 878-881.

Hirose, T., Bystricky, M., Kunze, K., et al. Semi-brittle flow during dehydration of lizardite-chrysotile serpentinite deformed in torsion: Implications for the rheology of oceanic lithosphere. Earth and Planetary Science Letters, 2006, 249(3-4): 484-493.

Holdsworth, R. E. Weak faults: Rotten cores. Science, 2004, 303: 181-182.

Hucka, V., Das, B. Brittleness determination of rocks by different methods. International Journal of Rock Mechanics and Mining Sciences & Geomechanics Abstracts, 1974, 11(10): 389-392.

Hull, J. Thickness-displacement relationships for deformation zones. Journal of Structural Geology, 1988, 10: 244-267.

Ingles, J. Terminations of ductile shear zones. Tectonophysics, 1986, 127(1-2): 87-95.

Ju, Y., Li, X., Ju, L., et al. Nanoparticles in the Earth surface systems and their effects on the environment and resource. Gondwana Research, 2022, 110: 370-392.

Ju, Y., Wang, G., Jiang, B. Microstructure analysis of the coal bed ductile shearing zone in the shallow level brittle deformation domain. Science in China (Series D), 2003, 3(7): 626-635 (in Chinese).

Keulen, N., Heilbronner, R., Stünitz, H., et al. Grain size distributions of fault rocks: a comparison between experimentally and naturally deformed granitoids. Journal of Structural Geology, 2007, 29(8): 1282-1300.

Krása, D., Wilkinson, C.D., Gadegaard, N., et al. Nanofabrication of two-dimensional arrays of magnetite particles for fundamental rock magnetic studies. Journal of Geophysical Research: Solid Earth, 2009, 114(B2): B02104.

Li, J., Cai, Z., Huang, Q., et al. Nanoparticles observed in a shear fracture of dolomite and a probable formation mechanism. Journal of Nanoscience and Nanotechnology, 2021, 21(1): 555-566.

Mair, K., Abe, S. 3D numerical simulations of fault gouge evolution during shear: Grain size reduction and strain localization. Earth and Planetary Science Letters, 2008, 274(1-2): 72-81.

Mamtani, M. A., Wenzel, O., Kontny, A., et al. "In-plane" site-specific FIB lamella extraction from deformed magnetite and the investigation of low angle grain boundaries under TEM. Journal of Structural Geology, 2023, 174: 104937.

McLaren, A. C., Pryer, L. L. Microstructural investigation of the interaction and interdependence of cataclastic and plastic mechanisms in feldspar crystals deformed in the semi-brittle field. Tectonophysics, 2001, 335(1-2): 1-15.

Means, W. D. Shear zones of types I and II and their significance for the reconstruction of rock history. Geological Society of America Bulletin, 1984, 16(1): 50.

Miranda, T. S., Neves, S. P., Celestino, M. A. L., et al. Structural evolution of the Cruzeiro do Nordeste shear zone (NE Brazil): Brasiliano-Pan-African ductile-to-brittle transition and Cretaceous brittle reactivation. Journal of Structural Geology, 2020, 141: 104203.

Mitra, G. Ductile deformation zones in blue ridge basement rocks and estimation of finite strains. Geological Society of America Bulletin, 1979, 90(10): 935-951.

Obert, L., Duvall, W. Rock Mechanics and the Design of Structures in Rock. New York, USA, Wiley, 1967.

Paterson, M. S. A high-pressure, high-temperature apparatus for rock deformation. International Journal of Rock Mechanics and Mining Sciences, 1970, 7(5): 517-526.

Ramsey, J. G. Folding and Fracturing of Rock. New York, USA, McGraw-Hill Book Company, 1968.

Sammis, C. G., Ben-Zion, Y. Mechanics of grain-size reduction in fault zones. Journal of Geophysical Research: Solid Earth, 2008, 113(B2): B02306.

Schleicher, A. M., van der Pluijm, B., Warr, L. N. Nanocoating of clay and creep of the San Andreas Fault at

Parkfield, California. Geology, 2010, 38(7): 667-670.

Siman-Tov, S., Aharonov, E., Sagy, A., et al. Nanograins form carbonate fault mirrors. Geology, 2013, 41(6): 703-706.

Smith, S. A. F., Billi, A., Di Toro, G., et al. Principal slip zones in limestone: Microstructural characterization and implications for the seismic cycle (Tre Monti Fault, Central Apennines, Italy). Pure and Applied Geophysics, 2011, 168(12): 2365-2393.

Stewart, M., Holdsworth, R. E., Strachan, R. A. Deformation processes and weakening mechanisms within the frictional-viscous transition zone of major crustal-scale faults: insights from the Great Glen Fault Zone, Scotland. Journal of Structural Geology, 2000, 22(5): 543-560.

Sun, S., Dong, Y. High temperature ductile deformation, lithological and geochemical differentiation along the Shagou shear zone, Qinling Orogen, China. Journal of Structural Geology, 2023, 167: 104791.

Sun, Y., Jiang, S., Zhou, W., et al. Nano-coating texture on the shear slip surface in rocky materials. Advanced Materials Research, 2013, 669: 108-114.

Sun, Y., Shen, X., Suzuki, T. Study on the ductile deformation domain of the simple shear in rocks - Taking brittle faults of the covering strata in the southern Jiangsu area as an example. Science in China (Series B), 1992, 35: 1512-1520.

Sun, Y., Shu, L., Lu, X., et al. Recent progress in studies on the nano-sized particle layer in rock shear planes. Progress in Natural Science, 2008a, 18(4): 367-373.

Sun, Y., Shu, L., Lu, X., et al. A comparative study of natural and experimental nano-sized grinding grain textures in rocks. Chinese Science Bulletin, 2008b, 53: 1217-1221.

Tian, P., He, C. Velocity weakening of simulated augite gouge at hydrothermal conditions: Implications for frictional slip of pyroxene-bearing mafic lower crust. Journal of Geophysical Research: Solid Earth, 2019, 124(7): 6428-6451.

Verberne, B. A., Plümper, O., Matthijs de Winter, D. A., et al. Superplastic nanofibrous slip zones control seismogenic fault friction. Science, 2014, 346: 1342-1344.

Viti, C., Collettini, C. Growth and deformation mechanisms of talc along a natural fault: A micro/nanostructural investigation. Contributions to Mineralogy and Petrology, 2009, 158(4): 529-542.

Viti, C., Hirose, T. Thermal decomposition of serpentine during coseismic faulting: nanostructures and mineral reactions. Journal of Structural Geology, 2010, 32(10): 1476-1484.

Watterson, J. Fault dimensions, displacement and growth. Pure and Applied Geophysics, 1986, 124(1): 365-373.

Wibberley, C. A. J., Shimamoto, T. Internal structure and permeability of major strike-slip fault zones: The median tectonic line in Mie Prefecture, southwest Japan. Journal of Structural Geology, 2003, 25(1): 59-78.

Zhan, L., Cao, S., Dong, Y., et al. Strain localized deformation variation of a small-scale ductile shear zone. Journal of Earth Science, 2023, 34(2): 409-430.